1

Band application of flue gas desulfurization gypsum improves sodic soils amelioration

Running head: Sodic soils amelioration with flue gas desulfurization gypsum

Wenchao Zhang[123], Wenxin Zhang[3※], Shujuan Wang[123], Jia Liu[24], Yan Li[123], Yuqun Zhuo[123],

Lizhen Xu[123], Yonggan Zhao[123*]

[1] Department of Energy and Power Engineering, Tsinghua University, Beijing 100084, China

[2] Beijing Engineering Research Centre for Ecological Restoration and Carbon Fixation of

Saline-Alkaline and Desert Land, Beijing 100084, China

[3] Shanxi Research Institute for Clean Energy of Tsinghua University, Shanxi 030032, China

[4] Tsinghua Agriculture Co., Ltd., Beijing 100084, China

* Corresponding author's email: Email: zhaoyonggan@tsinghua.edu.cn

12

---

[1] This author contributed equally to this work.

4

13 **Abstract:**

14 Blending flue gas desulfurization (FGD) gypsum with surface sodic soil is a universally

15 recognized method for the rapid amelioration of sodic soils; however, there are few reports on

16 whether other application methods (band application) will reclaim sodic soil. Three FGD

17 gypsum application methods, single-band application, dual-band application and blending,

18 were carried out using sodic soil in soil bins to investigate the effects of application method

19 on the wetting front, major cation concentrations and exchangeable sodium percentage (ESP)

20 during the process of water infiltration and in the soil profile after infiltration. The results

21 showed that the wetting fronts in the band treatments were denser in the horizontal direction

22 than in the vertical direction, but the blend treatment only had vertical migration. The main

23 channel of stream in the band treatments was concentrated below the application site of FGD

24 gypsum. The orders of desalting capacity were blend treatment, dual-band treatment and

25 single-band treatment for the same volume of outlet water. The dual-band treatment

26 significantly decreased the soil ESP of the whole soil bin, while the single-band treatment

27 only effectively reclaimed half of the soil. In the blend treatment, the ESP was 21.32% and

28 34.66% at depths of 30–35 cm and 35–40 cm and was close to zero at a depth of 0–30 cm.

29 Compared with blend treatment, band treatments have the advantage of long-term

30 amelioration of local sodic soil, and the performance is mainly affected by the Ca^{2+} pathway.

31 **Keywords:** Band application; flue gas desulfurization gypsum; pore channel; wetting front;

32 exchange reaction; Ca^{2+} pathway

5

1 Introduction

One of the greatest challenges in agriculture is the amelioration of sodic soils due to the huge area covered by such soils and restrictions on agricultural development in arid and semi-arid areas (Daliakopoulos et al., 2016; Haider, 2013). Sodic soil generally contains large amounts of Na^+, CO_3^{2-} and HCO_3^-. Na^+ adsorbed by soil colloids has hydrophilic properties, which can reduce the stability of soil aggregates in sodic soils by dispersing inorganic colloids in the narrow joints of soil particles and forming a soil layer with poor water permeability (Bagarello et al., 2006). On the other hand, Colloids adsorbed by Na^+ are more easily transported into pore spaces after rainfall and irrigation. When water flow is stagnant, hydrophilic colloids will gather to clog the pore throats caused by hydrodynamic bridging and size exclusion (Ramachandran, 2000), reducing the permeability of the soil (Carstens et al., 2017).Moreover, the high concentrations of CO_3^{2-} and HCO_3^- in sodic soil also result in a strongly alkaline pH (more than 8.5) (Fotovat and Naidu, 1998; Sakai et al., 2010). Previous studies have shown that in solutions of low ionic strength (IS) and high pH, the colloids adsorbed in the primary energy minimum are released into the bulk solution, which reduces the adsorption capacity of the colloids and increases the capability of colloidal migration (Yuan et al., 2020).

Increasing IS or adding high-valent cations (e.g., Ca^{2+}, Mg^{2+}, and Fe^{3+}) can promote adsorption by porous media and flocculation of colloids to form aggregates (McNew and LeBoeuf, 2016; Torkzaban et al., 2015). As its main component is $CaSO_4$, flue gas desulfurization (FGD) gypsum is a widespread, environmentally friendly and efficacious saline-alkali soil conditioner (Amezketa et al., 2005; Clark et al., 2001; DeSutter and Cihacek,

55 2009; Sakai et al., 2010; Wang and Yang, 2018). Dissolved Ca^{2+} from FGD gypsum reacts

56 with CO_3^{2-} and HCO_3^- and replaces exchangeable Na^+ in soil colloids to lower soil pH.

57 Additionally, Ca^{2+} promotes flocculation of colloids, which in turn increases the permeability

58 of sodic soils and the leaching of Na^+. As a consequence, the soil physical and chemical

59 properties of sodic soil are improved (Chen, 2011; Liao et al., 2019; Mao et al., 2016; Tirado-

60 Corbalá et al., 2019; Zhao et al., 2019).

61   To effectively ameliorate saline-alkali soil, FGD gypsum is commonly applied by even

62 mixing with topsoil (blend application) (Liao et al., 2019; Yu et al., 2014; Zhao et al., 2018).

63 However, the blending method accelerates the dissolution rate of FGD gypsum, leading to

64 large amounts of salt being released. Especially under rainfall or irrigation conditions, the

65 rapid dissolution of FGD gypsum may also lead to the loss of Ca^{2+} due to water leaching or

66 drainage (Zhao et al., 2019). This loss shortens the duration of saline-alkali soil amelioration

67 by FGD gypsum. In contrast, FGD gypsum can also be applied in a strip (band application).

68 Theoretically, band application can reduce the dissolution rate of FGD gypsum, release Ca^{2+}

69 slowly, decrease extra salt stress and prolong the improvement time compared with blending.

70 Applying concentrated FGD gypsum in the band method can be used to achieve the same

71 amelioration effect by adjusting the application rate and spacing between strips. In fact, band

72 application has been used in sunflower fields in recent years, but there are few related reports.

73 In addition, the differences in the amelioration effects between these two methods of FGD

74 gypsum application remain to be verified. According to these problems, we designed a soil

75 bin experiment to analyse the effect of band application of FGD gypsum on sodic soil by

76 observing the ion transport, exchange reaction process, reclamation effect and Ca^{2+} loss under

77　band application. In the experimental process, we explain water and salt migration in terms of

78　Ca^{2+} pathways, and relevant information is provided.

79　　　The application of FGD gypsum will change the infiltration path of irrigation water in

80　sodic soil, which will lead to differences in the distribution of saline and alkali parameters

81　after infiltration. Therefore, we hypothesized that 1) different application methods of FGD

82　gypsum can lead to a difference in the effect of the soil profile on sodic soil amelioration and

83　2) the effect of FGD gypsum on sodic soil amelioration is determined by the Ca^{2+} pathway.

84　Thus, a soil bin experiment was conducted to investigate these conjectures by monitoring the

85　variations in the wetting front, major cation concentrations in the leachate and ESP after

86　applying FGD gypsum.

87　**2 Materials and methods**

88　**2.1 Sodic soil and FGD gypsum**

89　Surface sodic soil with a depth of 20 cm was taken from Taonan District, Baicheng City, Jilin

90　Province, China (N45°14′24.08″, E123°35′38.75″). The soil samples were dried, crushed and

91　then screened through a 2 mm standard sieve. FGD gypsum collected from the Jilin Longhua

92　(Baicheng) coal-fired power plant was sequentially air-dried, ground fine with a grinding rod,

93　and screened to 100 mesh. The physical and chemical properties of the initial sodic soil and

94　FGD gypsum used in this study are shown in **Table 1**.

95　**2.2 Experimental design and implementation**

96　The four soil bins used for the experiment were made of plexiglass; two bins were 80 cm in

97   length, 60 cm in depth and 14.5 cm in width (bins 1 and 2), and bins 3 and 4 were 20 cm in

98   length, 60 cm in depth and 14.5 cm in width (Figure 1). At the bottom of the bins, there were

99   two layers of nylon nets (aperture of 0.125 mm) and an interlayer of quartz sand (particle size

100   of 0.18 mm) with a depth of 1 cm between the nylon layers. The bottom nylon net was used to

101   prevent quartz sand from leaking out from the outlet. The function of the quartz sand was to

102   prevent the migration of fine particles in the sodic soil from blocking the outlets. The upper

103   layer of nylon was used to separate the quartz sand layer from the layer of sodic soil. The

104   treated sodic soil was layered into the soil bins so that the bulk density of each layer with a

105   depth of 5 cm was 1.5 g cm^{-3}, and the bins were loaded to a depth of 40 cm.

106   In soil bin 1, a trench with a width of 6 cm and a depth of 5 cm was dug on one side 10

107   cm from the left edge. After adding 360 g FGD gypsum to the trench, the FGD gypsum was

108   covered with sodic soil; this system acted as the single-band treatment. In soil bin 2, two

109   trenches with a width of 4 cm and a depth of 5 cm were dug on two sides, both 10 cm from

110   the edge. After adding 180 g FGD gypsum to the two trenches and being and covered with

111   sodic soil, the system acted as the dual-band treatment. In soil bin 3, the 20-cm surface layer

112   of sodic soil was fully mixed with 90 g FGD gypsum and then compacted; this system acted

113   as the blend treatment. The soil bin with the above specifications was selected for blend

114   treatment because there was no difference in the horizontal migration of Ca^{2+} since the surface

115   soil layer was evenly blended with FGD gypsum. In soil bin 4, no FGD gypsum was added,

116   which acted as the control treatment (CK).

117   After the sodic soil and FGD gypsum were filled into the bins, the nylon net-quartz sand-

118   nylon net layers were laid on the soil surface to maintain the same horizontal osmotic

119 potential on the surface and prevent erosion from the addition of ultrapure water.

120 Subsequently, ultrapure water was added to ensure that the water depth was always 3 cm

121 above the soil surface. Cellophane was pasted on one side of the soil bins to draw wetting

122 fronts. At the beginning of the experiment (day 1), the time interval for drawing wetting fronts

123 should be 10, 20, or 30 minutes. When infiltration is slow (> 1 d), drawing a line every other

124 day is needed. In addition, when the EC of the outflow became steady, the addition of

125 ultrapure water was stopped, and the reclaimed soil was collected 2 d after water infiltration.

126 The four treatments were replicated three times. Finally, average values of all indicators were

127 used in the data analysis.

128 **2.3 Sampling and measurements**

129 At the beginning of the experiment, the wetting fronts in the soil bins were plotted, and the

130 corresponding time was recorded. The obtained wetting fronts in the three treatments were

131 scanned into JPG images by a printer. GetData software (GetData Pty Ltd, Kogarah NSW

132 2217, Australia) was used to determine the penetration depths in the wetting fronts.

133 When the leachate began to flow out of the outlet, the leachate was continuously

134 collected in beakers, and the volumes and times of the samples were recorded. Samples were

135 transferred to 100 mL plastic bottles and refrigerated. Before determining the chemical

136 properties of the water samples, the samples were filtered through a 0.45 μm membrane. pH

137 and EC were measured using digital FE-20 and FE-38 EC meters (Mettler Toledo

138 International Trade (Shanghai) Co., Ltd., China), respectively. Fifty millilitres of 25 leachate

139 samples at different stages were transferred into beakers. The samples were dried in an oven,

140 and the salt weight was weighed. The EC in the leachate was converted to salt concentration

141 based on the relationship between EC and solute (Figure 2). The concentrations of K^+, Na^+,

142 Ca^{2+} and Mg^{2+} in the leachate were measured using inductively coupled plasma atomic

143 emission spectrometry (ICP-AES, Prodigy-7, Leeman Labs Inc., Hudson, NH, USA).

144   The treated soils at a depth of 0–40 cm 2 d after water infiltration were collected by a

145 shovel. For a depth of 0–30 cm, layers 20 cm in length, 14.5 cm in width and 10 cm in depth

146 were collected. For soil at a depth of 30–40 cm, soils were sampled every 5 cm depth with a

147 length of 20 cm and width of 14.5 cm. The collected soil samples were air dried, mixed and

148 ground to a size fine enough to pass through a 2-mm sieve before soil analyses. The EC, pH,

149 and soluble cations were measured using 1:5 water extracts. The determination methods of

150 EC, pH and soluble ion concentrations were the same as those used for leachate

151 measurements. Exchangeable K^+, Na^+, Ca^{2+} and Mg^{2+} were extracted with ammonium acetate,

152 and their concentrations were measured using ICP-AES. The ESP was calculated using the

153 method described by Zhao et al. (2019).

154 **2.4 Data analysis**

155 A nonlinear regression equation was fitted to analyse the relationship between seepage

156 velocity and soil depth over time. To observe the migratory path of Ca^{2+}, the concentrations of

157 exchangeable and soluble Ca^{2+} and Na^+ in various soil layers were plotted as thermal pictures

158 by using GraphPad Prism 7.0 (GraphPad Software, LLC, San Diego, CA 92108, United

159 States).

3 Results

3.1 Water infiltration

3.1.1 Wetting front

Four representative wetting fronts and seepage velocities for four treatments are shown in Figure 3. In the single-band treatment, the wetting front was mainly distributed on the left side (0–40 cm) of the soil. The gap between the wetting fronts was larger in the vertical direction but denser in the horizontal direction. In the dual-band treatment, the right side was denser than the left side. The gap between wetting fronts in the blend treatment was large.

The seepage velocities of the four treatments increased following a power function. The CK had no leachate and the lowest seepage velocity throughout the entire experiment (75 d), and its fitting function was $Y_{CK}=5.632X^{0.399}$ and $R^2=0.949$ (Y_{CK} represents soil depth; X represents time.). The four treatments had the fastest penetration in the 0–20 cm soil layer, but the soil permeability began to decline gradually at 20–40 cm. In general, the order of seepage velocity was blend, single-band, dual-band (left), dual-band (right) and CK.

3.1.2 Seepage velocity and salinity in the leachate

The leachates in the single-band, dual-band and blend treatments started to flow out at 19.8, 13.9 and 0.3 d, respectively, after adding ultrapure water (Figure 4a). In the early period of leachate flow, the velocity of the blend treatment reached 3 L d^{-1}. After 0.49 d, the flow rate gradually stabilized at 0.2 L d^{-1}. In the dual-band treatment, the flow velocity of the leachate was low at the early stage (0.6 L d^{-1}), gradually increased to 1.5 L d^{-1} and finally decreased to 0.9 L d^{-1} at 69 d. The initial flow velocity in the single-band treatment was 0.6 L d^{-1}, and the

181   velocity decreased to 0.3 L d^{-1} after 69 d.

182   The salt concentration in the three treatments decreased substantially in the early stage

183   and gradually levelled off with increasing time (Figure 4b). Generally, the salt concentration

184   in the initial leachate of the blend treatment was twice that in the leachate of the dual-band

185   treatment, and it was the lowest in the single-band treatment. The salt concentration of the

186   leachate in the blend treatment gradually stabilized after 0.49 d. The rate of salt leaching in

187   the dual-band and single-band treatments gradually stabilized after 69 d.

188   **3.1.3 Na$^+$ and Ca^{2+} concentrations in the leachate**

189   The concentrations of Na$^+$ and Ca^{2+} in the leachate are shown in Figure 5. The concentrations

190   of Na$^+$ and Ca^{2+} in the leachate of the blend treatment were highest in the initial stage in all

191   three treatments. After 0.49 d, the Na$^+$ concentration tended to be stable.

192   The Na$^+$ concentration in the initial outflow of the dual-band treatment was

193   approximately half that of the blend treatment. After 16.9 d, the Ca^{2+} concentration in the

194   dual-band treatment decreased to 0, and the Na$^+$ concentration became steady. After 41.59 d,

195   the Ca^{2+} concentration showed a gradually increasing trend. The Na$^+$ concentration dropped

196   below 0.1 mol L^{-1}.

197   The concentrations and the decrease rates of Na$^+$ and Ca^{2+} in the single-band treatment

198   were the lowest and slowest among the three treatments. The Na$^+$ concentration in the single-

199   band treatment reached a steady flow rate after 38.56 d. In addition, the Ca^{2+} concentration

200   increased from zero to higher values after 54.07 d, and the Na$^+$ concentration was lower than

201   0.1 mol L^{-1}.

202   The chosen first inflection point was the mutation point of the critical exudation rate of

203 Na$^+$ in the three treatments, which was determined according to the point where the Na$^+$

204 concentration decreased to a steady rate. The second inflection point was determined

205 according to the Ca^{2+} concentration. The second inflection point was marked at the moment

206 when Ca^{2+} from the FGD gypsum flowed out with the leaching water. Therefore, the positions

207 of the first inflection point for the single-band, dual-band and blend treatments were 38.56 d,

208 16.9, and 0.49 d, respectively, and the positions of the second inflection point in the single-

209 band and dual-band treatments were 54.07 d and 41.59 d, respectively. The blend treatment

210 exhibited no second inflection point.

211 **3.2 Treated soil chemical properties**

212 **3.2.1 Soil pH and EC**

213 The soil pH and EC in the four treatments are shown in Figure 6. The pH in CK had no

214 obvious difference across the soil layers. In the single-band and dual-band treatments, the pH

215 was higher at distances farther from the application site of FGD gypsum. The pH value in the

216 0–40 cm soil layer of the blend treatment ranged from 7.78 to 9.12. In the single-band, dual-

217 band and blend treatments, the areas with a pH less than 9 accounted for 59.4%, 87.5% and

218 75%, respectively.

219 The EC in CK increased with soil depth. Except for the high EC values at the application

220 sites of FGD gypsum in the band treatments, the distribution of EC in other soil layers was

221 similar to that of pH. In the blend treatment, the EC was 166.5 mS cm^{-1} in the surface layer

222 (0–10 cm), then increased and subsequently decreased with increasing soil depth.

223 3.3.2 Soluble Na⁺ and Ca²⁺ concentrations

224 The distributions of soluble Na^+ and Ca^{2+} concentrations in the reclaimed soil are shown in

225 Figure 7. Na^+ in CK migrated downward, and the concentration reached a maximum at a

226 depth of 30–35 cm. In the single-band treatment, the soluble Na^+ concentration in the left

227 portion of soil (0–40 cm) was significantly higher than that in the right portion of soil (40–80

228 cm).The soluble Na^+ concentration in the dual-band treatment was significantly lower than

229 that in the single-band treatment, especially far from the application site of FGD gypsum. In

230 the blend treatment, the soluble Na^+ in the surface layer (0–10 cm) was the lowest.

231 3.3.3 Exchangeable Na⁺ and Ca²⁺ concentrations

232 The distribution of exchangeable Na^+ and Ca^{2+} concentrations and ESP in the reclaimed soil

233 are shown in Figure 8. In the single-band treatment, the exchangeable Na^+ concentration in

234 the soil below the site of FGD gypsum application 0–40 cm in the horizontal direction was

235 significantly lower than that of the soil on the right side (40–80 cm). The distribution of

236 exchangeable Ca^{2+} was contrary to that of Na^+. The Ca^{2+} concentration increases of 32% to

237 156% compared with that of the initial sodic soil.

238 The exchangeable Na^+ concentration in the dual-band treatment was lower than that in

239 the single-band treatment and was less than 0.5 cmol kg^{-1} in 88% of the soil. The

240 exchangeable Ca^{2+} concentration increase ranging from 65% to 166% over that of the initial

241 sodic soil.

242 In the blend treatment, the exchangeable Na^+ concentration was close to 0 at a soil depth

243 of 0–30 cm and was 3.60 cmol kg^{-1} at 35-40 cm, close to the initial value of the sodic soil.

244 The distribution of exchangeable Ca^{2+} showed an opposite trend from that of Na^+.

245   ESP in CK remained high value at a depth of 10–40 cm. The average ESPs in the single-

246 band, dual-band and blend treatments were 12.43%, 2.24% and 11.23%, respectively. On the

247 right side (40–80 cm) of the soil in the single-band treatment, the ESP was over 15%. ESP in

248 the dual-band treatment was less than 15%. In the blend treatment, the ESP at a soil depth of

249 0–30 cm was close to 0, and at a soil depth of 30–40 cm, it was close to that of the initial soil.

250 **4 Discussion**

251 **4.1 The process by which Ca^{2+} dissolved from FGD gypsum permeates soil layers**

252 The levels of ESP and pH and the concentration of soluble Na^+ were lower in the surface soil

253 (0–20 cm) than at deeper depths in the three treatments. The reason for this phenomenon was

254 that on the surface of the soil where FGD gypsum was applied, part of the Ca^{2+} dissolved

255 from the FGD gypsum exchanged with Na^+ in the surface sodic soil, resulting in the leaching

256 of Na^+ by the seepage effect. Another reason was that ions migrate to deeper soil layers with

257 ultrapure water according to the CK results, but this effect was limited. Low pH caused by the

258 reaction of CO_3^{2-} and HCO_3^- with Ca^{2+} to produce insoluble $CaCO_3$.

259   The blend treatment had the fastest seepage velocity, followed by the single-band, dual-

260 band (left), and dual-band (right) treatments. The transport of dissolved Ca^{2+} from FGD

261 gypsum is affected by the potential of gravity and osmosis. The presence of Ca^{2+} enlarged the

262 channel size by promoting colloidal agglomeration and increasing the permeability of the

263 surface soil (Sakai et al., 2010; Wang et al., 2013; Wang et al., 2008; Zhao et al., 2020), which

264 rapidly formed predominantly vertical downward channels caused by the low potential of

265 horizontal osmosis.

266   In the single-band and dual-band treatments, the seepage velocities in the horizontal

267 direction were slow. When the wetting front in the vertical direction in the single-band

268 treatment arrived at the bottom, there was also a horizontal osmotic potential towards the

269 right, so partially dissolved Ca^{2+} was transported in the horizontal direction. However, when

270 the wetting fronts on the two sides of the dual-band treatment overlapped each other, the

271 horizontal osmotic potential in the upper layer of the soil disappeared. As a result, more Ca^{2+}

272 migrated downward. This process also explains why leachate appeared sooner in the dual-

273 band treatment than in the single-band treatment. In addition, the different wetting fronts on

274 the two sides of the dual band treatment might be due to slight differences in the bulk density

275 of the soil layer during filling. In the blend treatment, there was only one-dimensional motion.

276 The micro-spaces occupied by dissolved FGD gypsum in the blended layer connect the pore

277 channels at the soil depth of 0–20 cm to form a pore network. Therefore, the seepage velocity

278 was the highest in this soil layer among the three treatments. The increase in Ca^{2+}

279 concentration at a depth of 20–30 cm demonstrated that Ca^{2+} migrated to 30–35 cm. In this

280 process, an intense exchange reaction between Ca^{2+} and Na^+ occurred along the wetting front.

281 **4.2 Main behaviour in the reclamation process**

282 When there was outflow from the soil, the IS in the leachate changed significantly. The Na^+

283 released in the initial stage of leachate flow was the dominant ion, so the trends of Na^+

284 concentration and EC were concordant.

285   The first stage ended when the concentrations of Na^+ in the single-band, dual-band and

286 blend treatments reached the first inflection point (38.56, 16.9, and 0.49 d). The EC values of

287 the three treatments were in the range of 10 to 11 mS cm^{-1}. Using sodium chloride solution as

288 a reference with an EC value of 10 mS cm^{-1}, the molality of sodium chloride at this time was

289 0.1 mol L^{-1}. The outflow velocity showed a downward trend. The decreased IS induced

290 colloidal migration, so blocking of the pore throats was responsible for these phenomena.

291 Significant amounts of colloids are rapidly released under reduced IS (Roy and Dzombak,

292 1996; Ryan, 1994). Most of the literature about colloidal release with reduced IS shows that a

293 decreased IS below a critical value leads to colloid release on account of reduction or

294 elimination of the secondary energy minimum (Ryan, 1994; Syngouna and Chrysikopoulos,

295 2015; Torkzaban. S; Kim H. N; Simunek, 2010). With the increase in IS to 0.1 M, colloid

296 immobilization (S$_f$) reached 1 (Bradford et al., 2012; Bradford et al., 2015). When the IS was

297 reduced from 0.1 M to zero, some colloids were released, (Torkzaban et al., 2015), and

298 outflowed (Bradford et al., 2015). Other evidence suggested that the critical salinity (i.e., the

299 EC associated with the critical salt concentration) for particle release was 7 mS cm^{-1}. When

300 the salinity changed abruptly, fine particles eluted from the soil column.

301   High IS can compress the electric double layer of colloids and porous media and

302 increase the attractive interaction between them (Bradford et al., 2015; Sasidharan et al.,

303 2014; Torkzaban et al., 2015; Kim H. N; Simunek, 2010). Hence, colloidal migration was

304 unlikely to occur in the first stage. In the second stage, the colloids adsorbed in the secondary

305 minimum were released into the solution due to decreased IS. When the colloids migrated to

306 the throat of the channel, physical blockage gradually reduced the velocity of the outflow. As

307 a result, the velocity decreased and reached a stable level. Notably, the Na$^+$ concentration in

308 the dual-band treatment showed a small peak during the period of 21–23 d, which might be

309   caused by the increase in Na^+ concentration along the channel after the solution penetrated

310   through the soil layer on the right side of the dual bands and mixing of the two channels

311   occurred. At the second inflection point, on account of decreased horizontal permeability and

312   the complete exchange of Ca^{2+} for Na^+ in the surrounding channels, some Ca^{2+} spread

313   vertically and flowed out of the soil with the water flow, resulting in a gradually increased

314   Ca^{2+} concentration. In addition, in the band treatments, the distribution of exchangeable Ca^{2+}

315   in the soil was uniform, and the concentration was approximately 2 times that of the original

316   sodic soil, which proved that the adsorption of Ca^{2+} had reached saturation. The blend

317   treatment did not reach the second inflection point, which was attributed to some Na^+ in the

318   bottom layer not being washed out by the exchange reaction.

319   The exchange reaction of K^+ and Mg^{2+} in soil is often neglected (Wang et al., 2013). The

320   concentrations of exchangeable K^+ and Mg^{2+} increased in the reclaimed soil and were more

321   evenly distributed (data not shown). The results showed that in the third stage of the

322   experiment, the exchangeable K^+ and Mg^{2+} all came from the FGD gypsum.

323   **4.3 Effects of the three application methods on the amelioration of sodic soil by FGD**

324   **gypsum**

325   All three application methods of FGD gypsum could reclaim sodic soil. Because of the low

326   solubility of FGD gypsum (approximately 2 parts per thousand at normal temperature), Ca^{2+}

327   could be continuously released into the soil water. Therefore, a large amount of FGD gypsum

328   can achieve the long-term amelioration of sodic soil.

329   In the absence of FGD gypsum (CK), Na^+ permeated with water and cause changes in

330   ESP, particularly at a depth of 0−10 cm. The distributions of soluble and exchangeable Na^+

331 and ESP in the band treatments indicated that the exchange reaction between Ca^{2+} and Na^{+}

332 and leaching of Na^{+} in the dual-band treatment were better than those in the single-band

333 treatment. The main channels were mainly concentrated in the vertical direction under the

334 areas where FGD gypsum was added. In addition, the buried FGD gypsum in the single-band

335 treatment had a pungent smell, which may be caused by hydrogen sulfide produced by

336 reduction in the absence of oxygen for a long time. The aqueous solution of hydrogen sulfide

337 is acidic and therefore lowers the pH of the soil. The effect of the single-band treatment in the

338 horizontal direction greater than 30 cm is unknown. The two bands of FGD gypsum with a

339 separation distance of 60 cm successfully remediated all of the soil in the bin. The advantages

340 of the band treatments were that they required little investment and released Ca^{2+} for the long

341 term. The blend treatment had advantages in terms of desalination, low water usage and a

342 high rate of alkali reduction; however, the high salt concentration in the leachate might cause

343 salt stress compared with band treatments. In addition, the soil at a depth of 30–40 cm still

344 had some soluble Na^{+}, which was consistent with the EC (4 μS cm^{-1}) in the leachate and pH

345 (9.54) and ESP (27.99%) in the reclaimed soil. The blend application of FGD gypsum

346 requires a large amount of manpower, material resources and funding support. An inadequate

347 amount of FGD gypsum would have anti-salt and anti-alkali effects.

348 **5 Conclusions**

349 In this study, three application methods of FGD gypsum were used to study the amelioration

350 of sodic soil. All application methods reclaimed sodic soil via different Ca^{2+} pathways. The

351 Ca^{2+} pathway, which was affected by soil moisture and gravitational potential, determined the

352   areas for amelioration. In the leachate of the blend treatment, a large amount of Na^+ was

353   released in a short time due to the high release velocity of effective Ca^{2+} and no horizontal

354   osmotic potential, while Na^+ was released slowly in the band treatments. The amelioration

355   areas of the single-band and dual-band treatments were mainly concentrated under the areas

356   where the FGD gypsum was placed. The application of a single band with excessive FGD

357   gypsum could effectively reclaim half of the total sodic soil in the bin, while the application

358   of dual bands reclaimed all of the sodic soil in the bin. In conclusion, the advantage of single-

359   band and dual-band treatments is their ability to reclaim sodic soil for a long time with simple

360   operation, in contrast to blend treatment.

361   **Acknowledgments**

368   **References**

369   Amezketa, E., Aragüés, R., & Gazol, R. (2005). Efficiency of sulfuric acid, mined gypsum,
370   and two gypsum by-products in soil crusting prevention and sodic soil reclamation.
371   Agronomy Journal. 97, 983–989.
372   Bagarello, V., Iovino, M., Palazzolo, E., Panno, M., & Reynolds, W.D. (2006). Field and
373   laboratory approaches for determining sodicity effects on saturated soil hydraulic
374   conductivity. Geoderma. 130, 1–13.

375   Bradford, S.A., Torkzaban, S., Kim, H., & Simunek, J. (2012). Modeling colloid and
376   microorganism transport and release with transients in solution ionic strength. Water
377   Resources Research. 48, W09509.
378   Bradford, S.A., Torkzaban, S., Leij, F., & Simunek, J. (2015). Equilibrium and kinetic models
379   for colloid release under transient solution chemistry conditions. Journal of Contaminant
380   Hydrology 181, 141–152.
381   Carstens, J.F., Bachmann, J., & Neuweiler, I. (2017). Effects of flow interruption on transport
382   and retention of iron oxide colloids in quartz sand. Colloids and Surfaces A:
383   Physicochemical and Engineering Aspects 520, 532–543.
384   Chen, C., Xu, X., Sadakata, M; Wang, S; Li, Y., & Li, Y. (2011). Use of the flue gas
385   desulfurization byproduct from thermal power plants and facilities and a method for
386   alkali soil amelioration. In: U.S. Patent (Ed.).
387   Clark, R.B., Ritchey, K.D., & Baligar, V.C. (2001). Benefits and constraints for use of FGD
388   products on agricultural land. Fuel 80, 821–828.
389   Daliakopoulos, I.N., Tsanis, I.K., Koutroulis, A., Kourgialas, N.N., Varouchakis, A.E.,
390   Karatzas, G.P., & Ritsema, C.J. (2016). The threat of soil salinity: A European scale
391   review. The Science of the Total Environment 573, 727–739.
392   DeSutter, T.M., & Cihacek, L.J. (2009). Potential agricultural uses of flue gas desulfurization
393   gypsum in the Northern Great Plains. Agronomy Journal 101, 817–825.
394   Fotovat, A., & Naidu, R. (1998). Changes in composition of soil aqueous phase influence
395   chemistry of indigenous heavy metals in alkaline sodic and acidic soils. Geoderma 84,
396   213–234.
397   Haider, M.Z., & Hossain, M. Z. (2013). Impact of salinity on livelihood strategies of farmers.
398   Journal of Soil Science and Plant Nutrition 13, 417–431.
399   Liao, R., Yu, H., Lin, H., & Yang, P. (2019). A quantitative study on three-dimensional pore
400   parameters and physical properties of sodic soils restored by FGD gypsum and leaching
401   water. Journal of Environment Management 248, 109303.
402   Mao, Y., Li, X., Dick, W.A., & Chen, L. (2016). Remediation of saline-sodic soil with flue gas
403   desulfurization gypsum in a reclaimed tidal flat of southeast China. Journal of
404   Environmental Sciences 45, 224–232.
405   McNew, C.P., & LeBoeuf, E.J. (2016). nC60 deposition kinetics: the complex contribution of
406   humic acid, ion concentration, and valence. Journal of Colloid and Interface Science
407   473, 132–140.
408   Ramachandran, V.F., & Scott Fogler, H. (2000). Plugging by hydrodynamic bridging during
409   flow of stable colloidal particles within cylindrical pores. Journal of Fluid Mechanics
410   385, 129–159.
411   Roy, S.B., & Dzombak, D.A. (1996). Colloid release and transport processes in natural and
412   model porous media. Colloids & Surfaces A: Physicochemical & Engineering Aspects
413   107, 245–262.
414   Ryan, J.N., & Gschwend, P.M. (1994). Effects of ionic strength and flow-rate on colloid
415   release - relating kinetics to intersurface potential-energy. Journal of Colloid & Interface
416   Science 164, 21–34.
417   Sakai, Y.J., Matsumoto, S., & Sadakata, M. (2010). Alkali soil reclamation with flue gas
418   desulfurization gypsum in China and assessment of metal content in corn grains. Soil

419 and Sediment Contamination: An International Journal 13, 65–80.

420 Sasidharan, S., Torkzaban, S., Bradford, S.A., Dillon, P.J., & Cook, P.G. (2014). Coupled
421 effects of hydrodynamic and solution chemistry on long-term nanoparticle transport and
422 deposition in saturated porous media. Colloids and Surfaces A: Physicochemical and
423 Engineering Aspects 457, 169–179.

424 Syngouna, V.I., & Chrysikopoulos, C.V. (2015). Experimental investigation of virus and clay
425 particles cotransport in partially saturated columns packed with glass beads. Journal of
426 Colloid and Interface Science 440, 140–150.

427 Tirado-Corbalá, R., Slater, B.K., Dick, W.A., Bigham, J., & Muñoz-Muñoz, M. (2019).
428 Gypsum amendment effects on micromorphology and aggregation in no-till Mollisols
429 and Alfisols from western Ohio, USA. Geoderma Regional 16, e00217.

430 Torkzaban, S., Bradford, S.A., Vanderzalm, J.L., Patterson, B.M., Harris, B., & Prommer, H.
431 (2015). Colloid release and clogging in porous media: Effects of solution ionic strength
432 and flow velocity. Journal of Contaminant Hydrology 181, 161–171.

433 Torkzaban. S; Kim H. N; Simunek, J.B., & Bradford, S. A. (2010). Hysteresis of colloid
434 retention and release in saturated porous media during transients in solution chemistry.
435 Environmental Science & Technology 44, 1662–1669.

436 Wang, J.M., Bai, Z.K., & Yang, P.L. (2013). Effect of byproducts of flue gas desulfurization
437 on the soluble salts composition and chemical properties of sodic soils. PLOS ONE 8(8),
438 e71011.

439 Wang, J.M., & Yang, P.L. (2018). Potential flue gas desulfurization gypsum utilization in
440 agriculture: A comprehensive review. Renewable and Sustainable Energy Reviews 82,
441 1969–1978.

442 Wang, S.J., Chen, C.H., Xu, X.C., & Li, Y.J. (2008). Amelioration of alkali soil using flue gas
443 desulfurization byproducts: productivity and environmental quality. Environmental
444 pollution 151, 200–204.

445 Yu, H.L., Yang, P.L., Lin, H., Ren, S.M., & He, X. (2014). Effects of sodic soil reclamation
446 using flue gas desulphurization gypsum on soil pore characteristics, bulk density, and
447 saturated hydraulic conductivity. Soil Science Society of America Journal 78, 1201–
448 1213.

449 Yuan, R.Q., Zhang, W.X., Tao, X., Wang, S.Q., & Zhang, L. (2020). Coupled effects of high
450 pH and chemical heterogeneity on colloid retention and release in saturated porous
451 media. Colloids and Surfaces A: Physicochemical and Engineering Aspects 586, 124285.

452 Zhao, Y.G., Wang, S.J., Li, Y., Liu, J., Zhuo, Y.Q., Chen, H.X., Xu, L.Z., & Sun, Z.T. (2018).
453 Extensive reclamation of saline-sodic soils with flue gas desulfurization gypsum on the
454 Songnen Plain, Northeast China. Geoderma 321, 52–60.

455 Zhao, Y.G., Wang, S.J., Li, Y., Zhuo, Y., Q., & Liu, J. (2019). Sustainable effects of gypsum
456 from desulphurization of flue gas on the reclamation of sodic soil after 17 years.
457 European Journal of Soil Science 70, 1082–1097.

458 Zhao, Y.G., Zhang, W.C., Wang, S.J., Liu, J., Li, Y., & Zhuo, Y.Q. (2020). Effects of soil
459 moisture on the reclamation of sodic soil by flue gas desulfurization gypsum. Geoderma
460 375, 114485.

461 Table 1

462 Physical and chemical properties of the initial soil and major components of the flue gas

463 desulfurization (FGD) gypsum used in this study.

EC (μS cm^{-1})	pH	ESP (%)	Bulk density (g cm^{-3})	Soil texture (g kg^{-1})		
				Sand	Silt	Clay
601.9	10.46	36.20	1.50	260	570	170

Ion content (cmol kg^{-1})							
	K	Na	Ca	Mg	Cl$^-$	SO$_4^{2-}$	CO$_3^{2-}$+HCO$_3^-$
Soluble ions	0.03	2.70	0.05	0.06	0.73	0.08	0.11
Exchangeable ions	0.14	3.58	2.58	1.00	–	–	–

Major components of the FGD gypsum (g kg^{-1})										
SO$_3$	CaO	CO$_2$	SiO$_2$	MgO	Na$_2$O	K$_2$O	N	F	Cl	Others
45.40	42.50	5.30	1.47	1.40	1.11	0.04	0.86	0.69	0.31	1.12

464 EC, electrical conductivity; ESP, exchangeable sodium percentage.

44
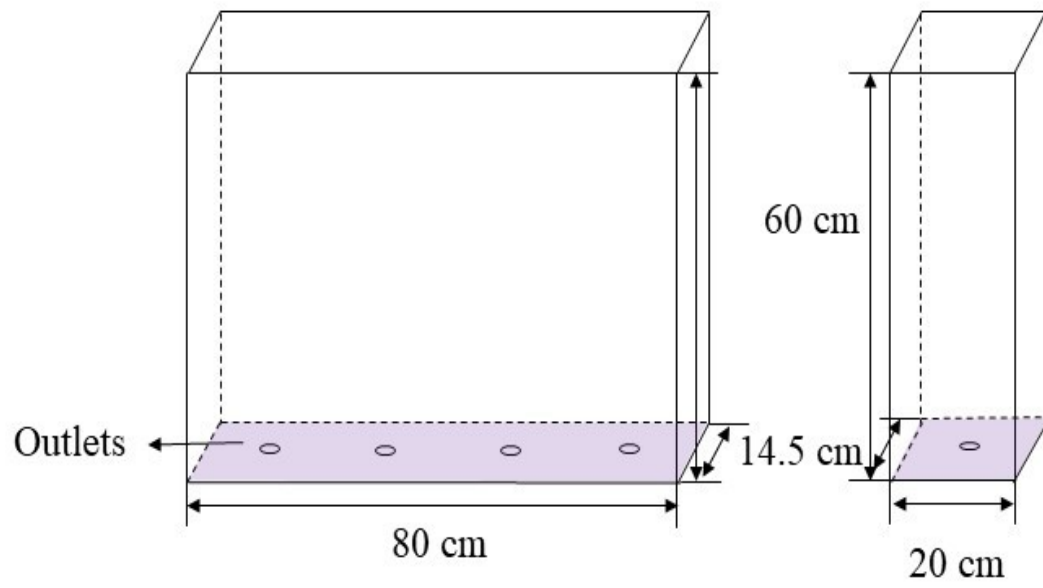
465

466 **Fig. 1.** Sketch of the soil bin used in this study.

45

y = 0.931x - 0.360
$R^2 = 0.999$
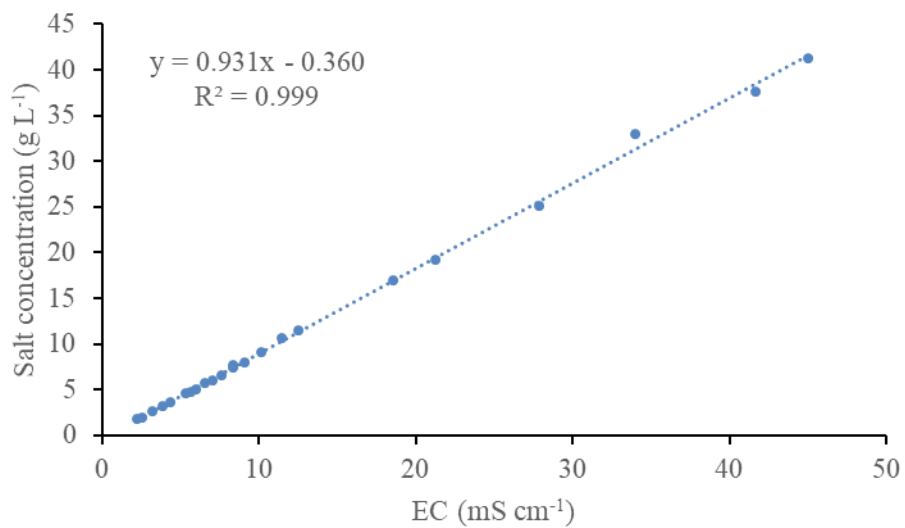
467

468 **Fig. 2.** Relationship between electrical conductivity (EC) and salt concentration in
469 lechate. y represents the salt concentration in lechate, g L^{-1}. x represents EC, mS cm^{-1}.

48

470

471

472
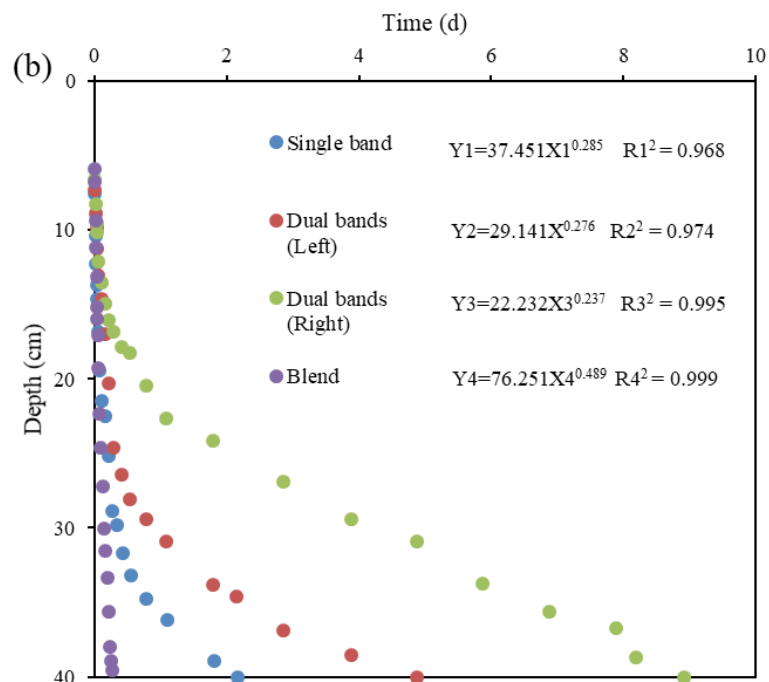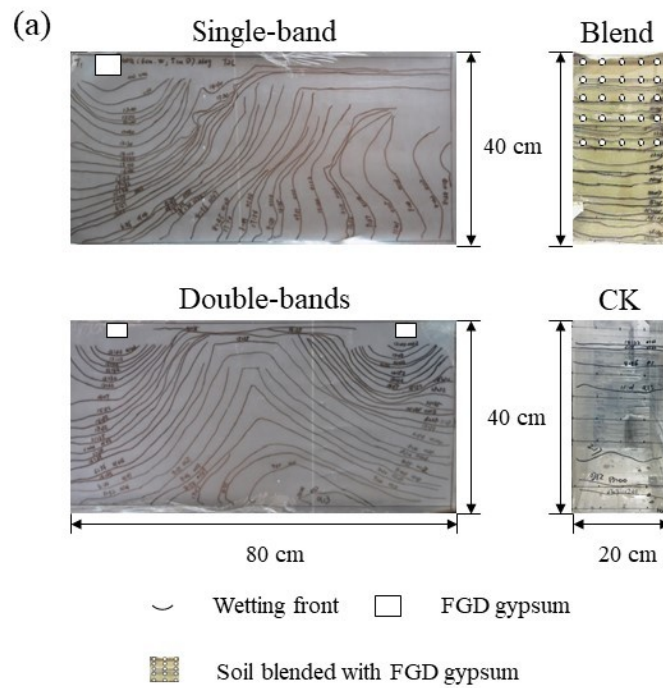
Fig. 3. Sketch of the wetting front (a) and seepage velocity (b) for different

treatments. Y_1, Y_2, Y_3 and Y_4 are fitting functions for the following treatments: single

49

50

475   band, dual bands (left), dual bands (right) and blend, respectively.
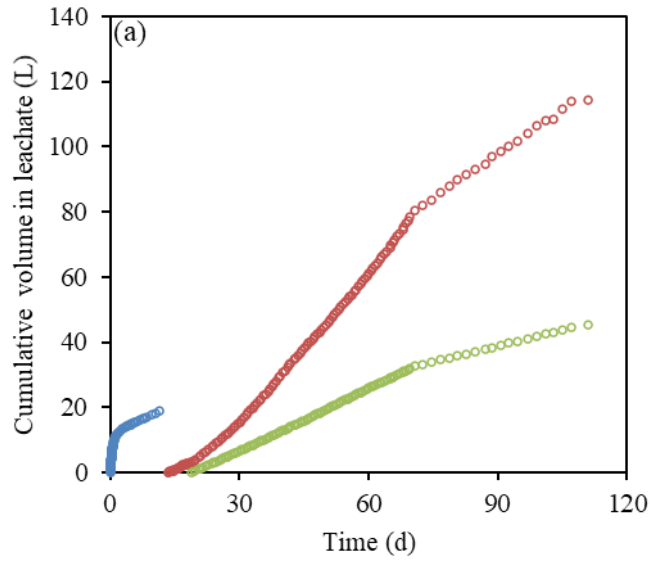
476
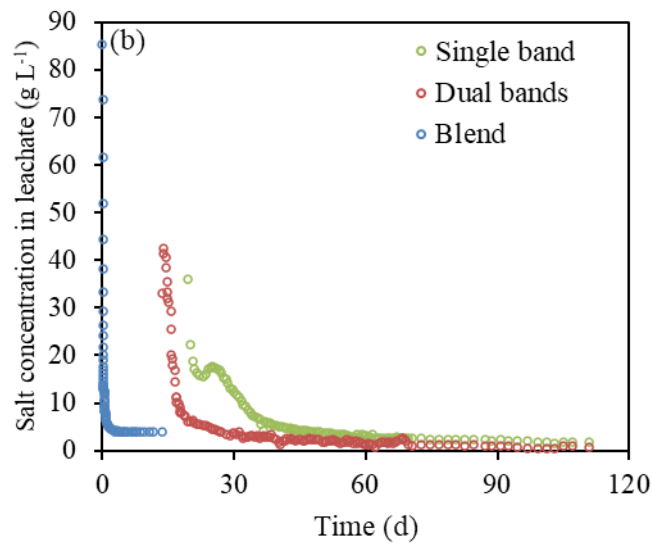
477

478 **Fig. 4.** Variation in the cumulative volume (a) and salt concentrations in leachate (b)

479 with time for different treatments.
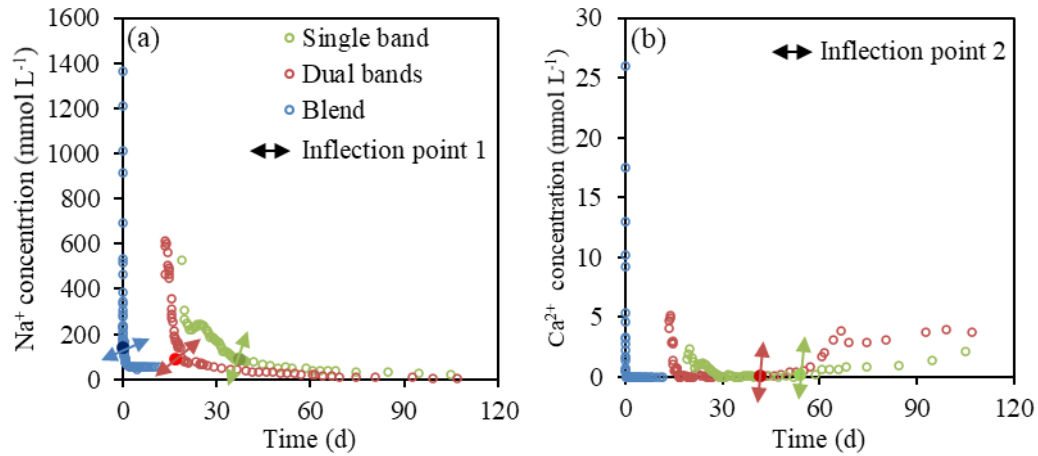
Fig. 5. Soluble Na$^+$ (a) and Ca^{2+} (b) concentrations of leachate with time for different treatments during the water infiltration process. Inflection point 1 indicates the point at which the concentration of Na$^+$ in the outflow decreases to a stable level. Inflection point 2 indicates the residual Ca^{2+} in the effluent are beginning to flow out; the blend treatment shows no such phenomenon.
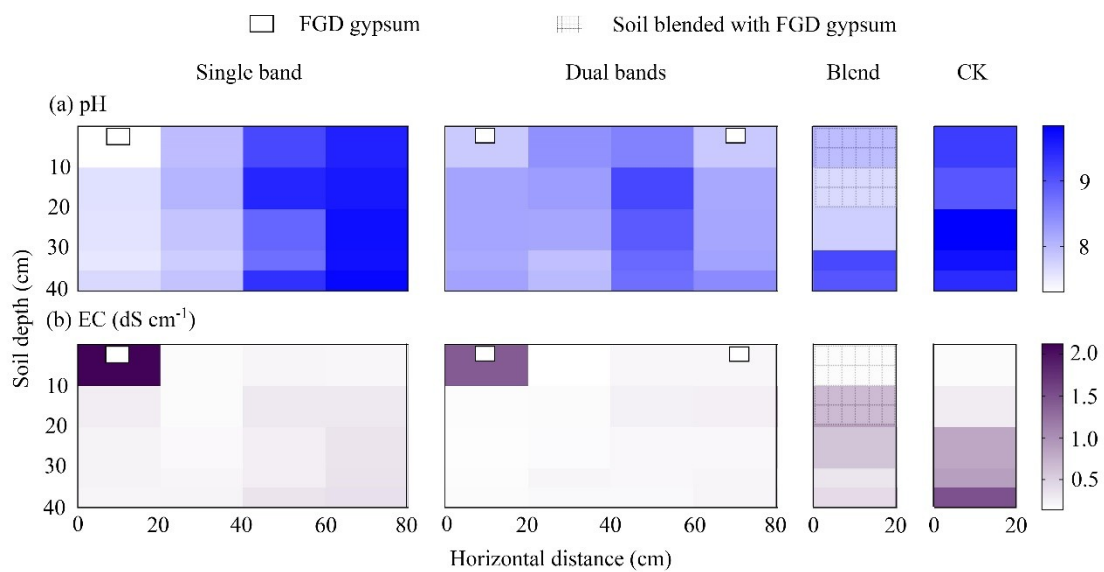
Fig. 6. Soil pH and electrical conductivity (EC) at a depth of 0-40 cm 2 days after water infiltration for different treatments.
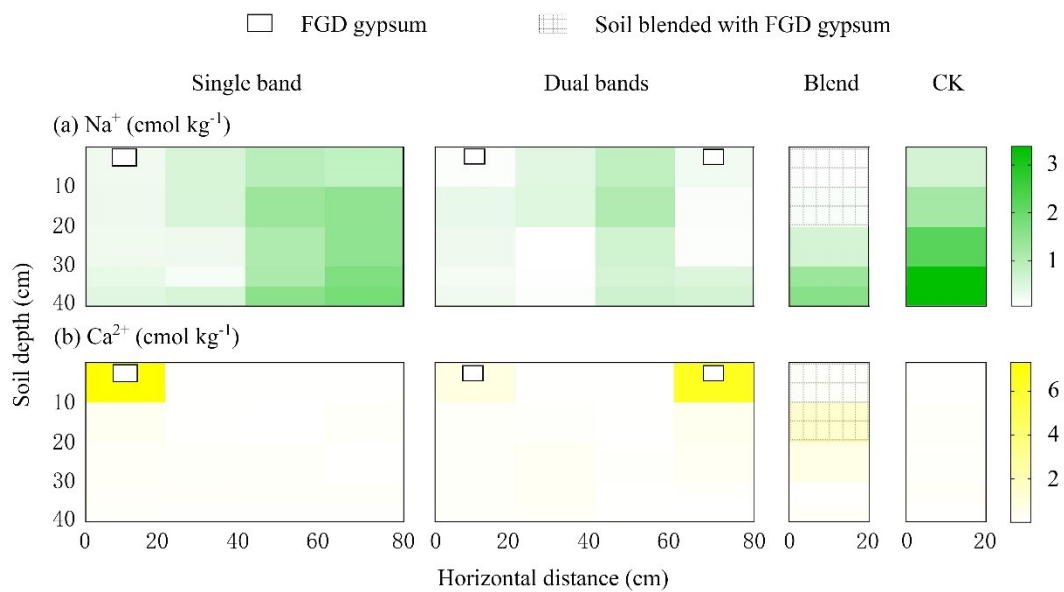
Fig. 7. Soluble Na^+ (a) and Ca^{2+} (b) in the reclaimed soils at a depth of 0–40 cm 2 days after water infiltration for different treatments.
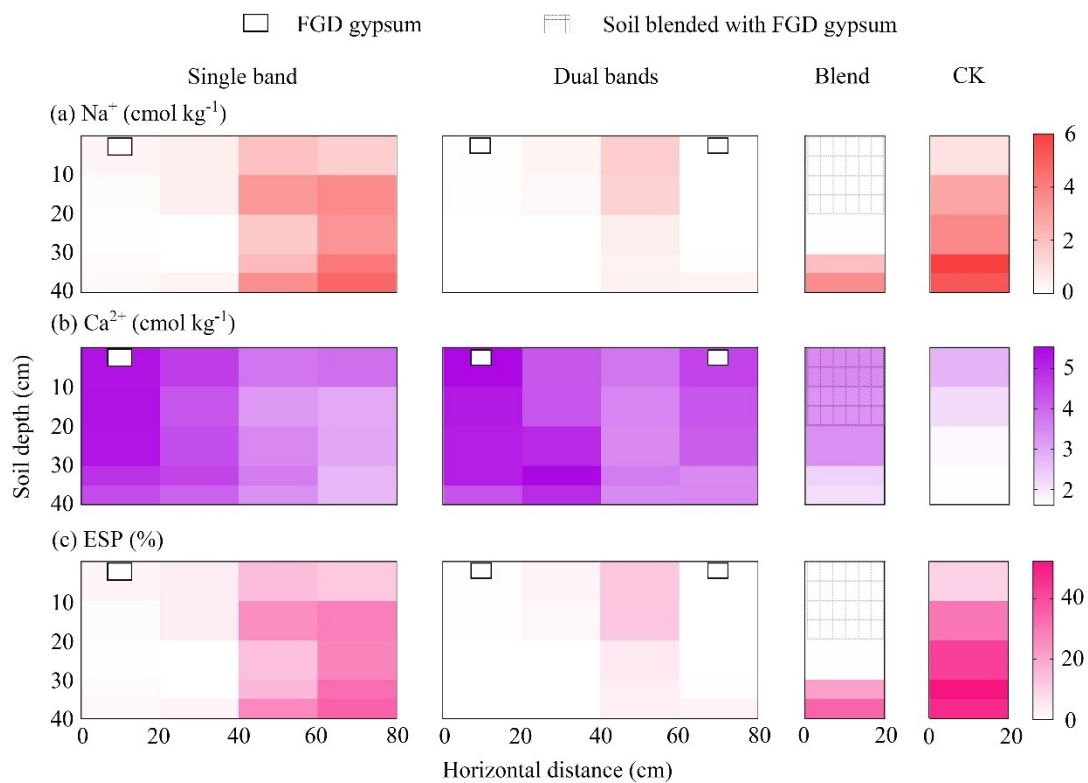
Fig. 8. Exchangeable Na$^+$ and Ca^{2+} and exchangeable sodium percentage (ESP) in the reclaimed soils at a depth of 0–40 cm 2 days after water infiltration for different treatments.